Journal of Biotechnology 274 (2018) 40–46

Contents lists available at ScienceDirect

Journal of Biotechnology

journal homepage: www.elsevier.com/locate/jbiotec

Spectroelectrochemical detection of microRNA-155 based on functional RNA immobilization onto ITO/GNP nanopattern

Mohsen Mohammadniaei[a], Jinho Yoon[a], Taek Lee[b], Jeong-Woo Choi[a,*]

[a] Department of Chemical and Biomolecular Engineering, Sogang University, 35 Baekbeom-ro (Sinsu-dong), Mapo-gu, Seoul 121-742, Republic of Korea
[b] Department of Chemical Engineering, Kwangwoon University, 20 Kwangwoon-Ro, Nowon-Gu, Seoul 01897, Republic of Korea

ARTICLE INFO

Keywords:
Spectroelectrochemical biosensor
microRNA detection
Surface enhanced Raman spectroscopy
Dynamic range extension
Single mismatch detection

ABSTRACT

We fabricated a microRNA biosensor using the combination of surface enhanced Raman spectroscopy (SERS) and electrochemical (EC) techniques. For the first time, the weaknesses of each techniques for microRNA detection was compensated by the other ones to give rise to the specific and wide-range detection of miR-155. A single stranded 3′ methylene blue (MB) and 5′ thiol-modified RNA (MB-ssRNA-SH) was designed to detect the target miR-155 and immobilized onto the gold nanoparticle-modified ITO (ITO/GNP). Upon the invasion of target strand, the double-stranded RNA transformed rapidly to an upright structure resulting in a notable decrease in SERS and redox signals of the MB. For the first time, by combination of SERS and EC techniques in a single platform we extended the dynamic range of both techniques from 10 pM to 450 nM (SERS: 10 pM–5 nM and EC: 5 nM–450 nM). As well, the SERS technique improved the detection limit of the EC method from 100 pM to 100 fM, while the EC method covered single-mismatch detection which was the SERS deficiency. The fabricated single-step biosensor possessing a good capability of miRNA detection in human serum, could be employed throughout the broad ranges of biomedical and bioelectronics applications.

1. Introduction

Cancer biomarkers, existed in tumor tissues or serum, comprise a wide range of molecules such as mRNA, DNA, cell receptors, enzymes and other metabolites (Sawyers, 2008). As the preliminary signs of the cancer, they play a significant role in the cancer detection at a very early-stage of the disease development (Wu and Qu, 2015). Amongst the others, microRNA (miRNA) as a short noncoding single-stranded RNA (18–25 nt) has attracted much interest for about a decade, ever since (Calin and Croce, 2006). They are transcribed from a long hairpin RNA called primary miRNA (pri-miRNA) with the help of different enzymes and proteins to eventually form the RNA-induced silencing complex (RISC) and further inactivate the mRNA of one or multiple genes (Krol et al., 2010). It has been recently proved that, altered expression level of miRNA can have serious consequences leading variety of diseases such as different types of cancers, diabetes, neurodegenerative diseases, cardiovascular disease, kidney and liver disease, etc. (Nalejska et al., 2014; Kato et al., 2013; de Planell-Saguer and Rodicio, 2013). As a result, precise detection of this important biomarker is highly demanded, although, their small size, low abundance and high homology have made it challenging to detect miRNAs in a very accurate and sensitive methodology.

Some well-known methods for the detection of oligonucleotides have been employed to detect miRNAs, including northern blotting (NB) (Válóczi et al., 2004), microarray (Li and Ruan, 2009) and quantitative reverse transcription polymerase chain reaction (qRT-PCR) (Halford, 1999). However, NB is a complex method which requires radiolabeling following by contamination and lower efficiency. Likewise, despite its sensitive detection, qRT-PCR still suffers from the detection of short strand oligonucleotides. Low melting temperature of the short targets makes the primer design very complicated and may causes cross-contamination and lower the sensitivity of the biosensor (Wu and Qu, 2015; Lee et al., 2014). Regarding the microarray technique, the main issue would be its high cost which makes this method less accessible to every user. To overcome the aforementioned limitations, some other signal amplification techniques (Chen et al., 2018a) were introduced such as, isothermal amplification (Zhang and Zhang, 2012), bio-barcode assay (Lee et al., 2014), nanoparticle-derived probes (Yin et al., 2012; Degliangeli et al., 2014), dichalcogenides based electrochemical biosensors (Wang et al., 2017), hybridization chain reaction (Chen et al., 2018b) and rolling cycle amplification-based methods (RCA) (Cheng et al., 2009). In spite of their high accuracy and pace, they are restricted to sequential process, using diverse enzyme and reagents also labor-intensiveness which impose cost and experimental

* Corresponding author.
E-mail address: jwchoi@sogang.ac.kr (J.-W. Choi).

https://doi.org/10.1016/j.jbiotec.2018.03.014
Received 27 December 2017; Received in revised form 2 March 2018; Accepted 23 March 2018
Available online 26 March 2018
0168-1656/

errors to the system. On the other hand, surface enhanced Raman spectroscopy (SERS) technique as a highly-efficient method to detect different types of biomarkers at a very low level of concentration has been also engaged for miRNA detection (Zhang et al., 2015a). However, because of the weak Raman scattering of oligonucleotides resulting from the poor scattering of ribose sugar and phosphate groups (Bell and Sirimuthu, 2006; Han et al., 2012), direct and one-step detection of single mutation in the target strand using SERS is still challenging (Zhang et al., 2015b; Wang et al., 2016; Song et al., 2016; Zhou et al., 2017). Accordingly, electrochemical biosensors (Drummond et al., 2003; Mohammadniaei et al., 2017; Shuai et al., 2017; Chen et al., 2017) have been introduced as the well-defined and cost-effective tools for the rapid detection of miRNAs and ability to detect single-mismatch mutations, however, their either need multistep detection process or have the reproducibility challenges (Liu et al., 2016; Labib et al., 2013; Campuzano et al., 2014). Hence, combination of two techniques might provide a credible platform to enhance the efficiency of miRNA biosensors.

To overcome those mentioned restrictions, here, we fabricated the MB-ssRNA-SH@ITO/GNP biosensor to detect miR-155 in a single-step fashion without the necessity for the additional enzymes and reagents using the combination of SERS and EC analysis (Tan et al., 2015). The miR-155 was found to be overexpressed in breast cancer cells (MDA-MB-231) and down regulated in lung cancer cells (A549) (Lee et al., 2014; Roa et al., 2010; Jiang et al., 2005). In a back-to-back supporting situation, which has not been reported elsewhere, SERS and EC techniques were combined to expand the dynamic range of the sensor from 10 pM to 450 nM. Moreover, based on this new approach, the weakness of SERS technique towards single base pair mutation was compensated by EC method, whilst the SERS measurement gave rise to the sensitivity and fidelity enhancement of miRNA detection. In this work, ITO substrate (conductive and transparent) was chemically modified by gold nanoparticle (ITO/GNP) to provide a GNP nanopattern solid substrate, since, the SERS-active patterns have proven to offer a higher signal stability than the liquid-form agents (Fig. 1). Methylene Blue (MB) was used as the simultaneous redox/Raman reporter (Xiao and Man, 2007; Kelley et al., 1997). Single-stranded RNA, which was complementary to the target RNA (miRNA), was commercially-modified at its both ends (3′-MB and 5′-thiol) and covalently immobilized onto the ITO/GNP substrate through its thiol group. In the presence of the target, a significant decrease in the spectroelectrochemical signals of the MB were observed resulting from the separation of MB from the ITO/GNP due to the pronounce decline in the surface plasmonic effect of GNPs and the electron transfer efficiency between MB and the electrode. The established biosensor was highly stable and showed a great selectivity towards detection of non-complementary miRNAs (miR-21, miR-141 and miR-143) and single mismatched targets.

2. Materials and methods

2.1. Materials and reagents

6-MHA (6-Mercaptohexanoic acid), RNase-free Phosphate buffered saline (PBS) (pH 7.4, 10 mM), (3-aminopropyl) triethoxysilane (APTES), Ethanol, Triton™ X-100, Sylgard® 184 Silicone Elastomer kit, phosphate buffer saline (PBS 7.4) and Tris (2-carboxyethyl) phosphine hydrochloride (TCEP) were purchased from Sigma-Aldrich (USA). 2 × 2 cm ITO glass (2 mm^2 active area) was purchased From G-mac (Korea). Gold nanoparticle (GNP, 10 nm) was purchased from BBI (UK). All other chemicals used in this study were of reagent grade and obtained commercially. Distilled and deionized (DI) water (resistance ≥ 18 MΩ) were produced using a Milli-Q® System (Millipore Corp.). All RNA oligonucleotides and DEPC-treated H_2O were provided from Bioneer® (Korea) as the following sequences:

MB-ssRNA-SH: 5′-Thiol / CCCCUAUCACGAUUAGCAUUAA / Methylene Blue -3′

miR-155: 5′- UUAAUGCUAAUCGUGAUAGGGG – 3′

1-Mis miR-155: 5′- UUAAUGCUA**G**UCGUGAUAGGGG – 3′

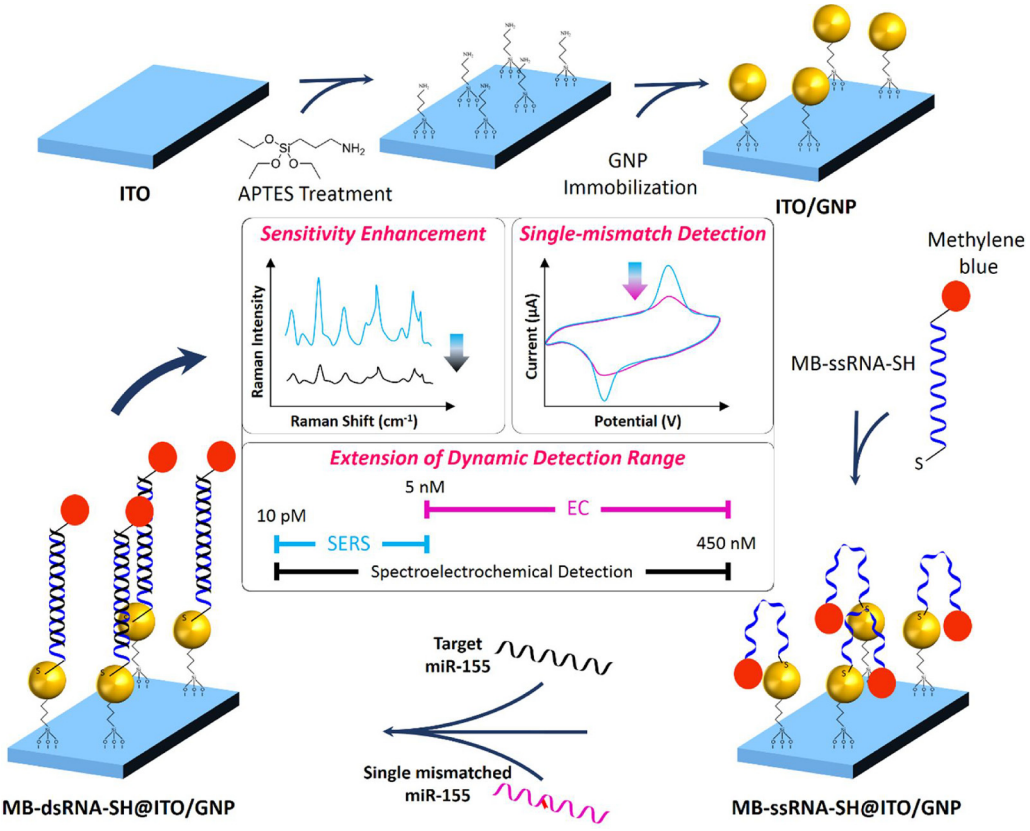

Fig. 1. Schematic diagram of electrode modification using ITO/APTES/GNP and further immobilization with methylene blue-modified dsRNA (MB-dsRNA-SH) for the sensitive and specific detection of miRNA-155 (For interpretation of the references to colour in this figure legend, the reader is referred to the web version of this article).

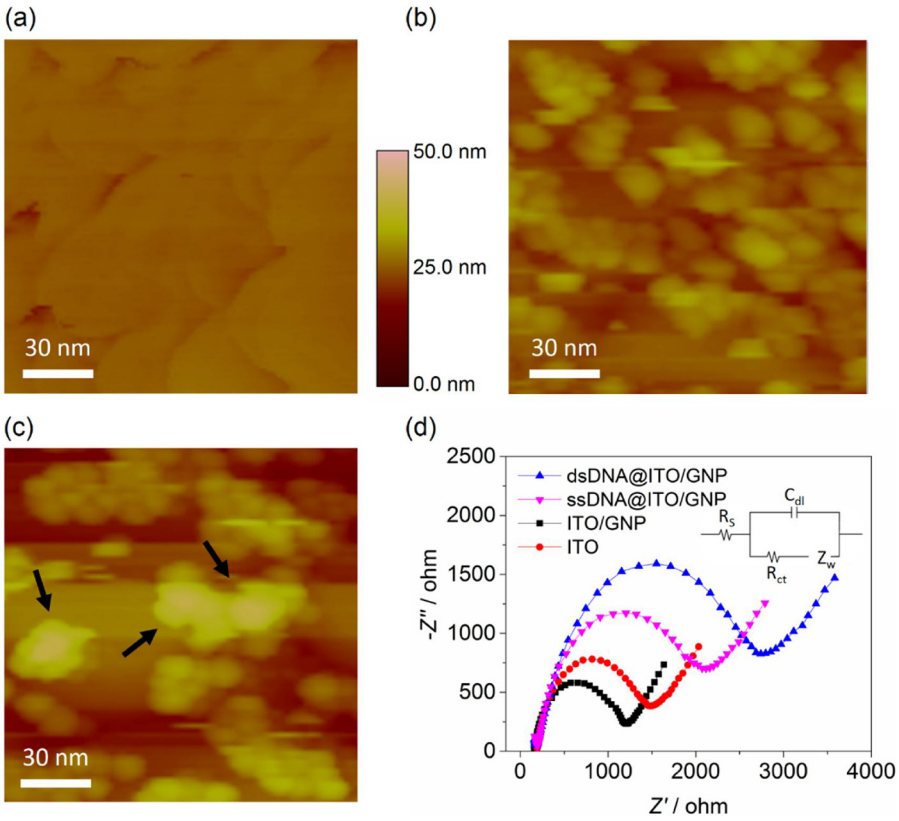

Fig. 2. Scanning tunneling microscopy (STM) analysis of the surface morphology of MB-dsRNA-SH@ITO/GNP biosensor. a) Bare ITO substrate, b) 10 nm GNP immobilized on ITO-modified APTES, c) MB-dsRNA-SH self-assembled on ITO/GNP substrate; black arrows show the location of final structures, d) Nyquist plots (Z′ vs. -Z″) obtained for bare ITO electrode, ITO/GNP, MB-ssRNA-SH@ITO/GNP and MB-dsRNA-SH@ITO/GNP. The inset shows the Randles equivalent circuit model; All the experiments were performed in PBS buffer (pH 7.4) containing 5 mM $Fe(CN)_6^{4-/3-}$.

* Mismatched nucleobase is underlined.
miR-21: 5′- UAGCUUAUCAGACUGAUGUUGA – 3′
miR-141: 5′- UAACACUGUCUGGUAAAGAUGG – 3′
miR-143: 5′- UGAGAUGAAGCACUGUAGCUCA – 3′

2.2. Fabrication of GNP-modified substrate

GNP modification of ITO was performed using our previous method (Kafi et al., 2016; Choi et al., 2016). ITO-coated glass substrates (G-mek, Korea) were cleaned sequentially using sonication for 30 min in 1% Triton X-100, DIW and ethanol. After washing process, to make the surface hydrophilic, the ITO substrates were directed to O_2 plasma for 5 min. Then, for silanization, ITO substrate was immersed into 5% APTES / 95% ethanol solution for 2 h at room temperature. After washing the surface with ethanol, the APTES-modified ITO substrates were heated at 99 °C for 20 min to cure the organosilane molecules. Afterwards, the 10 nm GNPs were dropped onto the APTES-modified ITO surface following to the incubation for 24 h at 4 °C. Finally, the GNP-modified substrate was rinsed with DEPC-treated water and dried using a stream of nitrogen to remove the unbound GNP.

2.3. Fabrication of MB-dsRNA-SH@ITO/GNP substrate

Substrate fabrication was done inside the clean bench to avoid RNA degradation. The MB-ssRNA-SH was treated with TCEP to avoid double thiol bindings. Then it was immobilized onto the GNP-modified ITO substrate at the concentration of 0.5 µM. After incubation for 24 h at 4 °C, substrate was rinsed with DEPC-treated water and dried by N_2 gas. In order to remove physically bound of MB-ssRNA-SH strands to the surface, the electrode was backfield by immersing into the solution of 10 mM 6-MHA for 2 h at 4 °C. After washing and drying process, the target RNA (miR-155 or others) was immobilized onto the surface at different concentrations and incubated for 2 h at RT. Then the sample was gently washed and dried and either implemented for experiment or kept at 4 °C in an appropriate dark humid chamber for further analysis.

2.4. Characterization of fabricated biosensor using scanning tunneling microscopy (STM)

The surface morphology of MB-dsRNA-SH@ITO/GNP electrode was analyzed using STM (Nanoscope IV/Multimode (Digital Instruments, USA)). Operating parameters for STM were chosen 0.999 Hz scan rate, 0.8 internal gain, 1.7 proportional gain at 1 nA current set point (Lee et al., 2010).

2.5. Electrochemical analysis method and SERS experiment

The SERS signal was measured on the hybrid substrate using confocal Raman spectroscopy (NTEGRA Spectra, NT-MDT) and a 785 nm near-infrared laser with 3 mW laser power on the sample plane. The intensity of the SERS spectra was measured from 10 different spots for three independent samples and the spectra were averaged. A home-made electrochemical chamber consisting of GNP/ITO as the working electrode, a platinum wire as the counter and Ag/AgCl as the reference electrode was fabricated. The cell chamber was attached to the GNP/ITO substrate by means of PDMS to simultaneously measure the Raman spectra and electrochemical behavior of the biosensor. The Raman spectrum was extracted from 10 points of at least 3 individual samples and the mean result was extracted and used. A blank spectrum was subtracted before each step. Cyclic voltammetry (CV) and EIS were performed using a CHI 660 A potentiostat (CH Instruments. Inc, USA.) equipped with general purpose electrochemical software and 10 mM PBS buffer at pH 7.4 was used as the electrolyte.

3. Results and discussion

3.1. Confirmation analysis of self-assembled MB-dsRNA-SH@ITO/GNP substrate

Layer-by-layer immobilization of MB-dsRNA-SH on ITO/GNP was investigated by scanning tunneling microscopy (STM) and

electrochemical impedance spectroscopy (EIS) analysis. Fig. 2a–c illustrates the topological image of the bare ITO surface, ITO/GNP and MB-dsRNA-SH @ITO/GNP. As it is shown in Fig. 2b, the size of the GNPs are around 10 nm and the height of ~ 12 nm. After treating the ITO/GNP substrate with MB-ssRNA-SH and miR-155, samples were directed for STM measurement (Fig. 2c). It is evidential that, there is a clear difference between the observed height of MB-dsRNA-SH@ITO/GNP (Fig. 2c, black arrows) and ITO/GNP (Fig. 2b). The height of the MB-dsRNA-SH@ITO/GNP structure was measured to be around 22 nm that confirms the upright position of the structure from which the 22 base pair RNA would be ~ 8 nm long.

EIS measurement was also performed to further understand the stepwise formation of the proposed biosensor platform. EIS is a useful technique for characterization of the formation of self-assembly monolayer biomolecules onto the electrode and to better disclose the electron transfer kinetics between the interfaces. The semicircular diameter of the Nyquist plot at higher frequencies explains the charge transfer resistance (R_{ct}) and its variation corresponds to the different modifications of the electrodes (Fig. 2d). All the measurements were conducted in a closed Faraday cage using a conventional three-electrode system in the frequency range of 100 kHz to 0.1 Hz at the potential and the AC amplitude of 5 mV in the PBS buffer (pH 7.4) containing 5 mM $[Fe(CN)_6]^{3-4-}$ redox probe. The data was fitted with Randle's model (Fig. 2d, inset) where R_S is the solution-phase resistance, C_{dl} is the double-layer capacitance and Z_W is the Warburg impedance. According to the obtained Nyquist diagrams in Fig. 2d, a semicircular diameter of $R_{ct} \approx 1284.3\ \Omega$ was observed for the bare ITO electrode and was decreased to ~ 1012.7 Ω after being modified by GNP. This shows the role of GNP in charge transfer rate enhancement between the redox probe and electrode. After immobilization of the ITO/GNP electrode with the MB-ssRNA-SH, the R_{ct} increased to ~ 1923.4 Ω due to the imposition of extra resistance to the electrode which damped the charge transfer rate between the interfaces and the solution; also the negative backbone of the ssRNA might electrostatically repel the negatively charged redox probe ($Fe(CN)_6^{3-4-}$). As seen, the R_{ct} increased again to ~ 2548.1 Ω, upon the hybridization of the modified electrode with the target miRNA strand. This may attributed to the weak conductivity of the RNAs as well as their natural negative charge to hinder electron transfer between the interfaces and redox probe. Therefore, the obtained EIS data alternatively proved the structural formation of the MB-dsRNA-SH@ITO/GP electrode.

3.2. Electrochemical performance of the MB-dsRNA-SH@ITO/GNP biosensor

In order to verify the electrochemical detection of miR-155 based on the MB-dsRNA-SH@ITO/GNP biosensor, cyclic voltammetry (CV) technique was utilized. The electrochemical detection mechanism was based on a signal-off method. The sensor probe consisted of MB-ssRNA-SH (complementary to miR-155) immobilized onto ITO/GNP nanopattern to be ready for the target invasion and detection. Methylene blue (MB) functioned as the redox signal reporter agent. Because of the high flexibility of single strand RNA (ssRNA), before the target hybridization, MB was in the closest distance to the ITO/GNP substrate (Schematic Fig. 1). This resulted in a high redox signal of MB due to the notable electron transfer efficiency between the electrode and MB (Fig. 3a, Off state). Accordingly, in the presence of the target strand (miR-155), the structure turns to the dsRNA and stayed in a well-defined upright position because of the firm structure of dsRNA compared to the ssRNA. Therefore, as it is evidential in Fig. 3a, the redox current peak of the MB significantly declined in the presence of miR-155 (On state). The reduction current peak of the MB was used as the detection signal of our biosensor.

Further, the developed biosensor performance was examined for single mismatch detection. In this regard, a strand of miR-155 having one single mismatch at the middle part was applied to the sensor. The statistical data in Fig. 3b describes the difference between the reduction current peak of MB obtained from the probe, perfectly-matched miR-155 and the 1-mismatched miR-155. As seen, the reduction current peak of the MB in the case of 1-mismatched miR-155 is about 5 times lower than that of the complementary-matched target due to the π-π orbital loss in dsRNA which interrupts the charge transfer from the electrode surface to MB through the double strand helix. The result which is in good agreement with the previous study (Inouye et al., 2005), well illustrates the high potency of the MB-dsRNA-SH@ITO/GNP biosensor towards single mutation detection of microRNA.

The dynamic range of the developed biosensor was also tested using CV technique. Fig. 3c indicates the cyclic voltammetric behavior of the MB upon different concentration of miR-155 target. As shown, the redox current peak of MB declined gradually as the concentration of miR-155 increased from 5 nM to 450 nM. The data confirmed that, the more target stands' concentration increased, the more MBs switched to the upright states resulting a gradual decline in the MB redox signal. The calibration curve (Fig. 3d) further confirmed the linear relationship between the target concentration and the redox current peak of MB under the regression equation of $I_{pc}\ /\mu A = -1.25 \times 10^{-3}\ C/nM + 9.6 \times 10^{-1}\ (R^2 = 0.994)$, where C is the concentration of miRNA. The detection limit for the electrochemical detection of miR-155 was calculated 100 pM possessing a dynamic detection range of 5 nM to 450 nM, which needed to be improved.

3.3. MicroRNA-155 detection using surface enhanced Raman spectroscopy (SERS)

To improve the performance of the proposed biosensor, SERS experiment was accomplished. We took the advantage of the capability of MB as a Raman dye and performed SERS experiment on the similar samples with same experimental conditions that we used for electrochemical analysis. The homemade electrochemical cell enabled us to measure SERS and CV on the same sample which was highly acquired to increase the detection fidelity. The Raman signals were recorded and averaged prior to any analysis. As seen in Fig. 4a (Off state), in the absence of target (biosensor probe), MB was at the closest position to the GNPs giving rise to the SERS spectra enhancement. This was due to the prominent surface plasmon resonance of the GNP which is because of the combined resonant oscillation of the free electrons of the conduction band in the noble metals leading a sharp and intense adsorption band through the visible region (Campion and Kambhampati, 1998). After the target (miR-155) hybridization, MB was detached from the GNP which was followed by a pronounce decrease in the Raman intensity signal (Fig. 4a, On state). As seen in Fig. 4a and inset, comparing to the Raman signal obtained from the complementary miR-155, hybridization of the biosensor with 1-mismatched miR-155 provided almost same results, demonstrating the deficiency of SERS technique to detect single base pair mutation. This is attributed to the fact that, the SERS signal of the target molecules/biomolecules can be only obtained when the target is in the close vicinity of the SERS-active nanostructure (Campion and Kambhampati, 1998). Since, hybridization of the biosensor with 1-mismatched miR-155 and complementary miR-155 resulted in the MB detachment from nanoparticle in a similar manner, identical Raman signals were observed.

The observed Raman bands at ~597, ~671, ~896, ~1157, ~1304 and ~1627 cm^{-1}, were originated from MB (Xiao and Man, 2007; Wong-ek et al., 2010; Pallaoro et al., 2013; Naujok et al., 1993), while the band recorded at ~ 812 cm^{-1} might due to the O—P—O stretching (Thomas et al., 1971; Thomas, 1970; Small and Peticolas, 1971; Leulliot et al., 1999a, b; Hernández et al., 2003; Benevides et al., 2005; Baumruk et al., 2001). A clear band at ~1045 cm^{-1} was seen which may be originated from P—O stretching and sugar phosphate of -C-O- bonding (Thomas, 1970; Guan and Thomas, 1996). The band at ~ 1460 cm^{-1} is reported to be dedicated to adenine-uracil base pairs (Thomas, 1970; Small and Peticolas, 1971; Baumruk et al., 2001) also

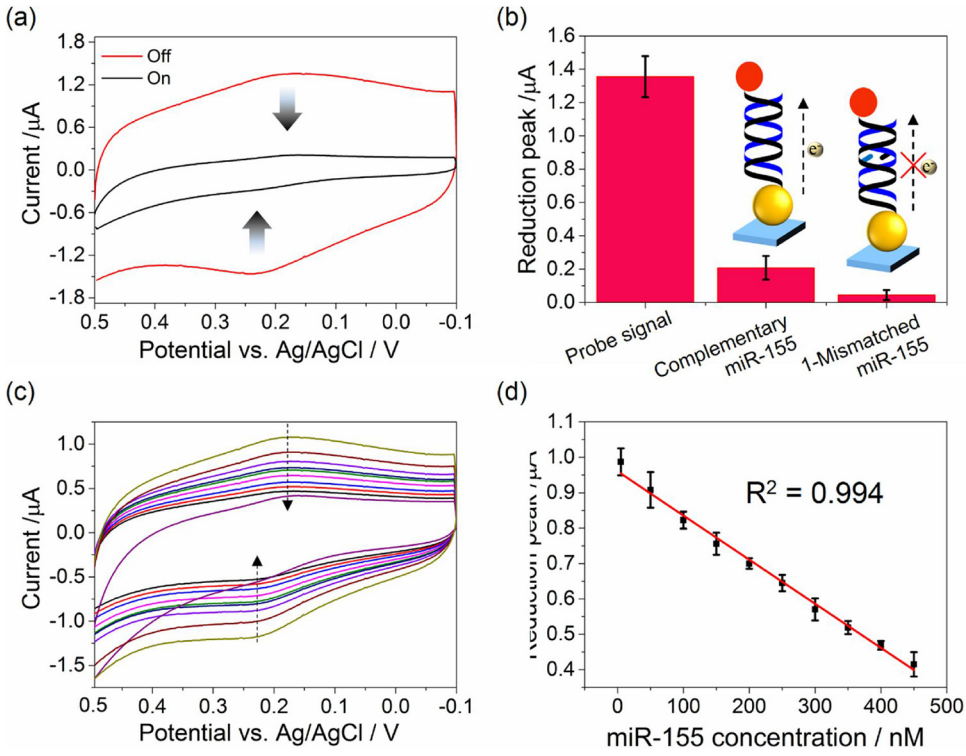

Fig. 3. Electrochemical analysis of sensor performance. a) Cyclic voltammograms obtained from MB-dsRNA-SH@ITO/GNP biosensor before (off) and after (on) miR-155 invasion at the concentration of 500 nM. b) Statistical analysis of the measured reduction peak variation of MB upon the introduction of complementary miR-155 and single-mismatched miR-155. c) Cyclic voltammograms of MB-dsRNA-SH@ITO/GNP in 10 mM PBS (pH 7.4) as a function of different concentration of miR-155 from 5 nM to 450 nM. d) Linear calibration curve resulting from the relationship between the observed reduction current peaks of Methylene blue and miR-155 concentration. All the electrochemical measurements were done at RT and the scan rate of 50 mV S^{-1}.

the Raman signal at ~ 1531 cm^{-1} is assigned to the adenine, guanine and cytosine stretching (Thomas, 1970; Small and Peticolas, 1971; Leulliot et al., 1999a, b; Baumruk et al., 2001). The Raman bands at ~597 and ~1627 cm^{-1} were seen to be more clear, however the high Raman intensity at ~597 cm^{-1} may be due to the florescence properties of the MB which provided a cone-shaped peak at that region.

The corresponding Raman maps of the On/Off states of the proposed biosensor is illustrated in Fig. 4b. A homogenous Raman map of 25 μm^2 was observed for both "On" and "Off" states. This shows the well distribution of sensor probe (MB-ssRNA-SH) on the surface and subsequent structural transformation to the upright position of almost all of the ssRNAs upon the target hybridization and formation of the

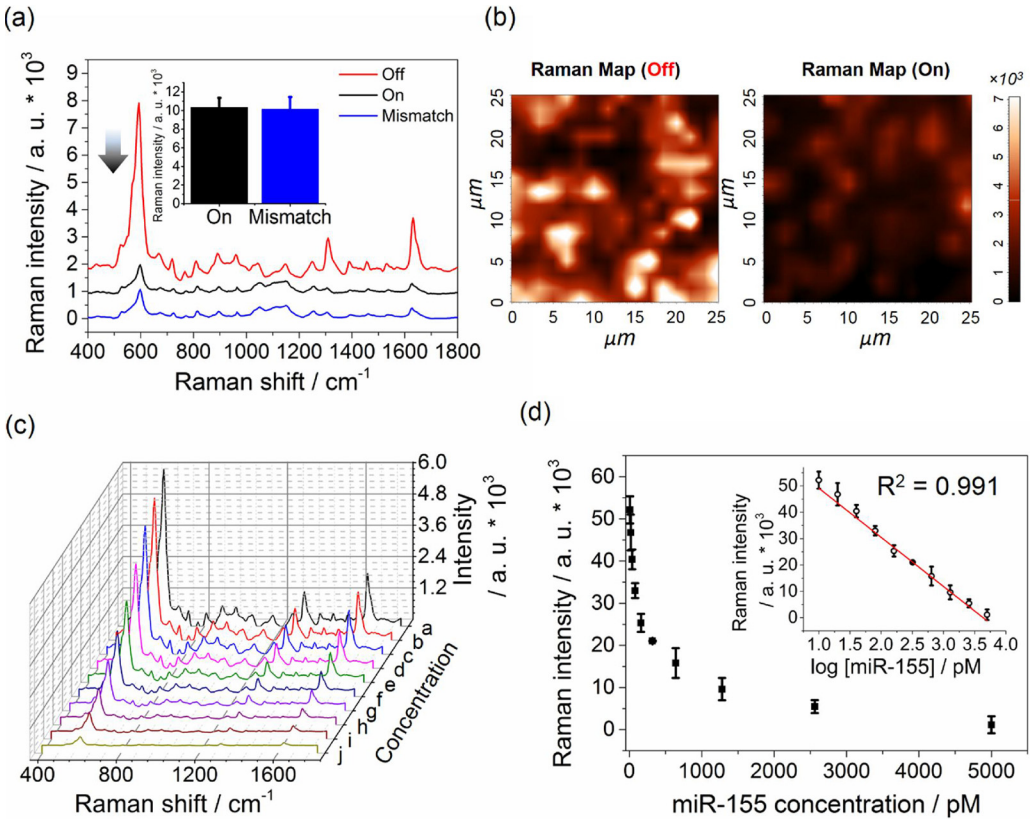

Fig. 4. Raman analysis of sensor performance. a) Typical SERS spectrum of MB-dsRNA-SH@ITO/GNP biosensor in the absence (Off) and presence (On) of 1 nM miR-155; Inset shows the statistical data for the Raman intensities recorded from the biosensor after being hybridized by complementary miR-155 (On) and 1-mismatched miR-155 (Mismatch), b) Corresponding Raman maps for the On/Off states. c) SERS spectra obtained from different concentrations of miR-155 (a: 10 pM, b: 20 pM, c: 40 pM, d: 80 pM, e: 160 pM, f: 320 pM, g: 640 pM, h: 1280 pM, i: 2560 pM, j: 5 nM). d) Calibration curve of the Raman intensity of MB-dsRNA-SH@ITO/GNP biosensor as a function of miR-155 concentration, inset shows linear relationship between Raman intensity and log concentration of miR-155. Experiments are done at 1 s exposure time and 785 nm laser. Both spectra are normalized for both laser power and exposure time. Data were collected based on three independent experiments and averaged over 40 random spots.

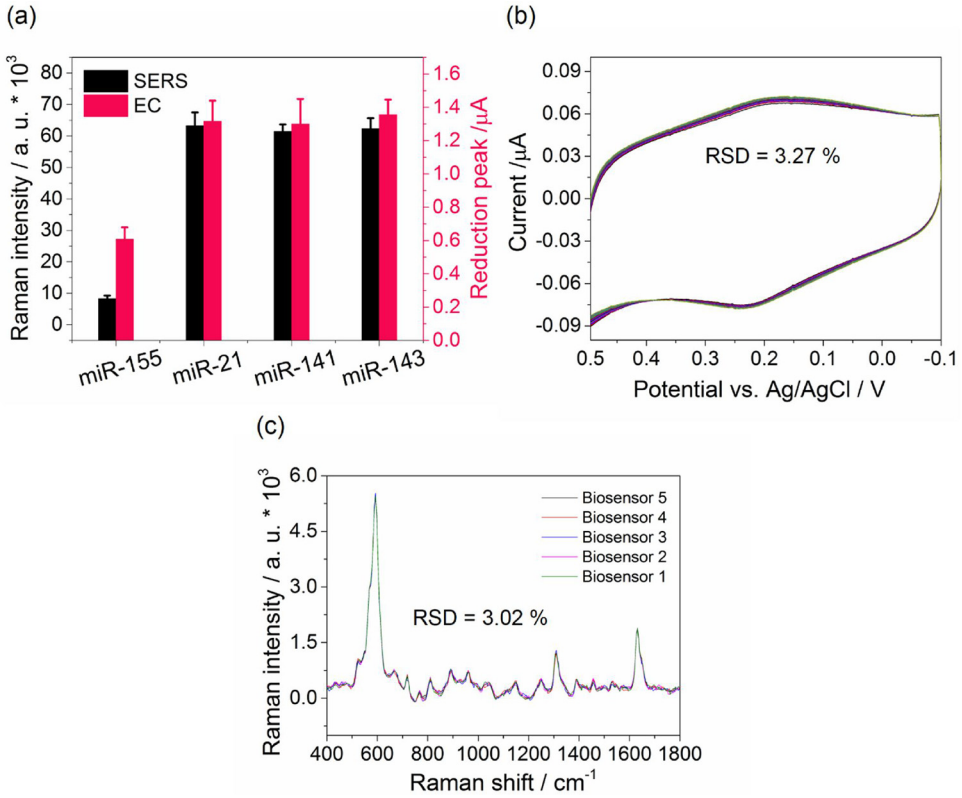

Fig. 5. Selectivity and stability investigation of the developed biosensor. a) Statistical analysis of the variation of Raman intensity of the developed biosensor and reduction current peak of MB upon the invasion of perfectly-matched miR-155 at the concentration of 1 nM and 300 nM for the SERS and EC measurements, respectively; and non-target strands (miR-21, miR-141 and miR-143) at 10-fold higher concentrations. b) 100 cycles of cyclic voltammograms obtained from MB-dsRNA-SH@ITO/GNP biosensor after the invasion of 200 nM miR-155 at the scan rate of 50 mV S^{-1}. Each 10 cycles increments are illustrated. c) SERS spectra of five different biosensors after detection of 20 pM miR-155.

Table 1
Determination of miRNA-155 concentration level in human serum.

Sample	Added (M)	Found (M)	Recovery (%)	RSD (%)
1	1×10^{-13}	0.969×10^{-13}	96.9	4.2
2	5×10^{-13}	5.165×10^{-13}	103.3	3.9
3	1×10^{-12}	0.952×10^{-12}	95.2	5.1

dsRNA. Fig. 4c plots the alteration of Raman intensity of the MB-dsRNA-SH@ITO/GNP biosensor as a function of miR-155 concentration, from which by increasing the target concentration the Raman signal decreased continuously. A linear relationship was observed (Fig. 4d) from the plot of Raman intensities as a function of miR-155 concentration. The dynamic detection range for the SERS measurement was 10 pM to 5 nM. Regression equation was $I/a.u. = -1.86 \times 10^4 \, Log \, C/pM + 6.71 \times 10^4$ ($R^2 = 0.991$) and the detection limit was measured to be 100 fM, considering the S/N = 3 method. As a result, spectroelectrochemical method assisted us to have a wide dynamic range of 10 pM to 450 nM which was safeguarded by both SERS and EC data in a back-to-back supporting situation.

3.4. Selectivity, stability and reproducibility of MB-dsRNA-SH@ITO/GNP biosensor

The selectivity of the proposed electrochemical biosensor was examined using different microRNA target strands (miR-21, miR-141 and miR-143). As it is evident in Fig. 5a, upon the addition of a non-target RNA strands to the sensor probe no significant drop was observed neither for SERS signal nor for the electrochemical signal of the MB.

Stability experiment was carried out using CV behavior of the MB-dsRNA-SH@ITO/GNP biosensor during 100 cycles of measurement (Fig. 5b). A very small decrease in MB redox current peaks were seen (RSD = 3.27%) owing to the strong bonding of the MB-ssRNA, ssRNA-SH and GNP/thiol. As for the repeatability test, 10 sensor probes at identical experimental conditions were directed to the CV and SERS measurement. The RSD was measured 4.2% and 3.6%, respectively. Also, after one week of storage of the as-prepared biosensors at 4 °C, the sensitivity of the biosensor did not change. After 3 weeks, the RSD was calculated 3.1% over its response to miR-155.

Furthermore, the feasibility of the fabricated biosensor towards miRNA detection inside the human serum was examined. Different concentration of miR-155 was added to the 5% serum and the prepared samples were directed to the sensor platform and the data was calculated based on the standard addition method. The results are tabulated in Table 1, showing a good recovery of 95.2%–103.3%, which indicates that the proposed biosensor is well capable in the determination of miRNA concentration level in real biological samples.

4. Conclusion

A microRNA biosensor composed of bi-functional RNA and GNP@ITO was fabricated for the spectroelectrochemical detection of miRNA-155 in a single-step fashion. The single stranded RNA, which was labeled by MB and thiol group at each ends and immobilized onto the ITO/GNP nanopattern substrate, provided a substantial spectroelectrochemical-active nanostructured biosensor. Having high self-folding tendency of ssRNA compared to ssDNA, the MB was held elegantly in the proper vicinity to the ITO/GNP resulting in a pronounce spectroelectrochemical signal which further dropped significantly upon the introduction of target stand. For the first time, by combination of SERS and EC methods we could widen the dynamic range of specific detection of miRNA in single step without the need for the additional enzymes and reagents, which was relayed from SERS to EC from 10 pM to 450 nM. Also the deficiency of SERS technique towards single mismatch detection of RNA/DNA was covered by EC method, whereas SERS supported the weakness of EC to enhance the sensitivity of our biosensor from 100 pM to 100 fM. Even though the proposed biosensor, with the capability of miRNA detection inside the human serum, does not offer the highest sensitivity, but, our novel approach for the combination of EC and SERS techniques to backfill each other's weaknesses

towards nucleic acid detection can be a stepping stone in upgrading former bioelectronic devices and developing various switchable devices.

Acknowledgements

This research was supported by the Leading Foreign Research Institute Recruitment Program, through the National Research Foundation of Korea (NRF), funded by the Ministry of Science, ICT and Future Planning (MSIP) (2013K1A4A3055268) and Basic Science Research Program through the National Research Foundation of Korea (NRF) funded by the Ministry of Education (2016R1A6A1A03012845) and by Nano·Material Technology Development Program through the National Research Foundation of Korea (NRF) funded by the Ministry of Science, ICT and Future Planning.(2009-0082580).

References

Baumruk, V., Gouyette, C., Huynh-Dinh, T., Sun, J.-S., Ghomi, M., 2001. Comparison between CUUG and UUCG tetraloops: thermodynamic stability and structural features analyzed by UV absorption and vibrational spectroscopy. Nucleic Acids Res. 29, 4089–4096.

Bell, S.E.J., Sirimuthu, N.M.S., 2006. Surface-enhanced Raman rpectroscopy (SERS) for sub-micromolar detection of DNA/RNA mononucleotides. J. Am. Chem. Soc. 128, 15580–15581.

Benevides, J.M., Overman, S.A., Thomas, G.J., 2005. Raman, polarized Raman and ultraviolet resonance Raman spectroscopy of nucleic acids and their complexes. J. Raman Spectrosc. 36, 279–299.

Calin, G.A., Croce, C.M., 2006. MicroRNA signatures in human cancers. Nat. Rev. Cancer 6, 857–866.

Campion, A., Kambhampati, P., 1998. Surface-enhanced Raman scattering. Chem. Soc. Rev. 27, 241–250.

Campuzano, S., Torrente-Rodríguez, R.M., López-Hernández, E., Conzuelo, F., Granados, R., Sánchez-Puelles, J.M., Pingarrón, J.M., 2014. Magnetobiosensors based on viral protein p19 for microRNA determination in cancer cells and tissues. Angew. Chem. Int. Ed. 53, 6168–6171.

Chen, Y.-X., Zhang, W.-J., Huang, K.-J., Zheng, M., Mao, Y.-C., 2017. An electrochemical microRNA sensing platform based on tungsten diselenide nanosheets and competitive RNA-RNA hybridization. Analyst 142, 4843–4851.

Chen, Y.-X., Huang, K.-J., Niu, K.-X., 2018a. Recent advances in signal amplification strategy based on oligonucleotide and nanomaterials for microRNA detection-a review. Biosens. Bioelectron. 99, 612–624.

Chen, Y.-X., Huang, K.-J., He, L.-L., Wang, Y.-H., 2018b. Tetrahedral DNA probe coupling with hybridization chain reaction for competitive thrombin aptasensor. Biosens. Bioelectron. 100, 274–281.

Cheng, Y., Zhang, X., Li, Z., Jiao, X., Wang, Y., Zhang, Y., 2009. Highly sensitive determination of microRNA using target-primed and branched rolling-circle amplification. Angew. Chem. Int. Ed. 48, 3268–3272.

Choi, J.-H., Lee, J., Shin, W., Choi, J.-W., Kim, H.J., 2016. Priming nanoparticle-guided diagnostics and therapeutics towards human organs-on-chips microphysiological system. Nano Convergence 3, 24.

de Planell-Saguer, M., Rodicio, M.C., 2013. Detection methods for microRNAs in clinic practice. Clin. Biochem. 46, 869–878.

Degliangeli, F., Kshirsagar, P., Brunetti, V., Pompa, P.P., Fiammengo, R., 2014. Absolute and direct microRNA quantification using DNA–gold nanoparticle probes. J. Am. Chem. Soc. 136, 2264–2267.

Drummond, T.G., Hill, M.G., Barton, J.K., 2003. Electrochemical DNA sensors. Nat. Biotechnol. 21, 1192–1199.

Guan, Y., Thomas, G.J., 1996. Vibrational analysis of nucleic acids. III. Conformation-dependent Raman markers of the phosphodiester backbone modeled by dimethyl phosphate. J. Mol. Struct. 379, 31–41.

Halford, W.P., 1999. The essential prerequisites for quantitative RT-PCR. Nat. Biotechnol. 17 835-835.

Han, X.X., Ozaki, Y., Zhao, B., 2012. Label-free detection in biological applications of surface-enhanced Raman scattering. TrAC Trends Anal. Chem. 38, 67–78.

Hernández, B., Baumruk, V., Leulliot, N., Gouyette, C., Huynh-Dinh, T., Ghomi, M., 2003. Thermodynamic and structural features of ultrastable DNA and RNA hairpins. J. Mol. Struct. 651–653, 67–74.

Inouye, M., Ikeda, R., Takase, M., Tsuri, T., Chiba, J., 2005. Single-nucleotide polymorphism detection with “wire-like” DNA probes that display quasi “on–off” digital action. Proc. Natl. Acad. Sci. U. S. A. 102, 11606–11610.

Jiang, J., Lee, E.J., Gusev, Y., Schmittgen, T.D., 2005. Real-time expression profiling of microRNA precursors in human cancer cell lines. Nucleic Acids Res. 33, 5394–5403.

Kafi, M.A., Cho, H.-Y., Choi, J.-W., 2016. Engineered peptide-based nanobiomaterials for electrochemical cell chip. Nano Convergence 3, 17.

Kato, M., Castro, N.E., Natarajan, R., 2013. MicroRNAs: potential mediators and biomarkers of diabetic complications. Free Radic. Biol. Med. 64, 85–94.

Kelley, S.O., Barton, J.K., Jackson, N.M., Hill, M.G., 1997. Electrochemistry of methylene blue bound to a DNA-modified electrode. Bioconj. Chem. 8, 31–37.

Krol, J., Loedige, I., Filipowicz, W., 2010. The widespread regulation of microRNA biogenesis, function and decay. Nat. Rev. Genet. 11, 597–610.

Labib, M., Khan, N., Ghobadloo, S.M., Cheng, J., Pezacki, J.P., Berezovski, M.V., 2013. Three-mode electrochemical sensing of ultralow microRNA levels. J. Am. Chem. Soc. 135, 3027–3038.

Lee, T., Kim, S.-U., Min, J., Choi, J.-W., 2010. Multilevel biomemory device consisting of recombinant azurin/cytochrome c. Adv. Mater. 22, 510–514.

Lee, H., Park, J.-E., Nam, J.-M., 2014. Bio-barcode gel assay for microRNA. Nat. Commun. 5, 3367.

Leulliot, N., Baumruk, V., Gouyette, C., Huynh-Dinh, T., Turpin, P.Y., Ghomi, M., 1999a. Aqueous phase structural features of GNRA tetraloops formed in short hairpins as evidenced by UV absorption and Raman spectroscopy. Vib. Spectrosc. 19, 335–340.

Leulliot, N., Baumruk, V., Abdelkafi, M., Turpin, P.Y., Namane, A., Gouyette, C., Huynh-Dinh, T., Ghomi, M., 1999b. Unusual nucleotide conformations in GNRA and UNCG type tetraloop hairpins: evidence from Raman markers assignments. Nucleic Acids Res. 27, 1398–1404.

Li, W., Ruan, K., 2009. MicroRNA detection by microarray. Anal. Bioanal. Chem. 394, 1117–1124.

Liu, S., Gong, H., Wang, Y., Wang, L., 2016. Label-free electrochemical nucleic acid biosensing by tandem polymerization and cleavage-mediated cascade target recycling and DNAzyme amplification. Biosens. Bioelectron. 77, 818–823.

Mohammadniaei, M., Lee, T., Yoon, J., Lee, D., Choi, J.-W., 2017. Electrochemical nucleic acid detection based on parallel structural dsDNA/recombinant azurin hybrid. Biosens. Bioelectron. 98, 292–298.

Nalejska, E., Mączyńska, E., Lewandowska, M.A., 2014. Prognostic and predictive biomarkers: tools in oersonalized oncology. Mol. Diagn. Ther. 18, 273–284.

Naujok, R.R., Duevel, R.V., Corn, R.M., 1993. Fluorescence and fourier transform surface-enhanced Raman scattering measurements of methylene blue adsorbed onto a sulfur-modified gold electrode. Langmuir 9, 1771–1774.

Pallaoro, A., Hoonejani, M.R., Braun, G.B., Meinhart, C., Moskovits, M., 2013. Combined surface-enhanced Raman spectroscopy biotags and microfluidic platform for quantitative ratiometric discrimination between noncancerous and cancerous cells in flow. J. Nanophoton. 7 073092-073092.

Roa, W., Brunet, B., Guo, L., Amanie, J., Fairchild, A., Gabos, Z., Nijjar, T., Scrimger, R., Yee, D., Xing, J., 2010. Identification of a new microRNA expression profile as a potential cancer screening tool. Clin. Invest. Med. 33, E124–E132.

Sawyers, C.L., 2008. The cancer biomarker problem. Nature 452, 548–552.

Shuai, H.-L., Huang, K.-J., Chen, Y.-X., Fang, L.-X., Jia, M.-P., 2017. Au nanoparticles/hollow molybdenum disulfide microcubes based biosensor for microRNA-21 detection coupled with duplex-specific nuclease and enzyme signal amplification. Biosens. Bioelectron. 89, 989–997.

Small, E.W., Peticolas, W.L., 1971. Conformational dependence of the Raman scattering intensities from polynucleotides. III. Order-disorder changes in helical structures. Biopolymers 10, 1377–1418.

Song, C.Y., Yang, Y.J., Yang, B.Y., Sun, Y.Z., Zhao, Y.P., Wang, L.H., 2016. An ultrasensitive SERS sensor for simultaneous detection of multiple cancer-related miRNAs. Nanoscale 8, 17365–17373.

Tan, Y., Yang, J., Xiang, K., Tan, Q., Guo, Q., 2015. Suppression of microRNA-155 attenuates neuropathic pain by regulating SOCS1 signalling pathway. Neurochem. Res. 40, 550–560.

Thomas, G.J., 1970. Raman spectral studies of nucleic acids. Biochim. Biophys. Acta, Nucleic Acids Protein Synth. 213, 417–423.

Thomas, G.J., Medeiros, G.C., Hartman, K.A., 1971. The dependence of Raman scattering on the conformation of ribosomal RNA. Biochem. Biophys. Res. Commun. 44, 587–592.

Válóczi, A., Hornyik, C., Varga, N., Burgyán, J., Kauppinen, S., Havelda, Z., 2004. Sensitive and specific detection of microRNAs by northern blot analysis using LNA-modified oligonucleotide probes. Nucleic Acids Res. 32 e175-e175.

Wang, H.-N., Crawford, B.M., Fales, A.M., Bowie, M.L., Seewaldt, V.L., Vo-Dinh, T., 2016. Multiplexed detection of MicroRNA biomarkers using SERS-based inverse molecular sentinel (iMS) nanoprobes. J. Phys. Chem. C 120, 21047–21055.

Wang, Y.-H., Huang, K.-J., Wu, X., 2017. Recent advances in transition-metal dichalcogenides based electrochemical biosensors: a review. Biosens. Bioelectron. 97, 305–316.

Wong-ek, K., Eiamchai, P., Horprathum, M., Patthanasettakul, V., Limnonthakul, P., Chindaudom, P., Nuntawong, N., 2010. Silver nanoparticles deposited on anodic aluminum oxide template using magnetron sputtering for surface-enhanced Raman scattering substrate. Thin Solid Films 518, 7128–7132.

Wu, L., Qu, X., 2015. Cancer biomarker detection: recent achievements and challenges. Chem. Soc. Rev. 44, 2963–2997.

Xiao, G.-N., Man, S.-Q., 2007. Surface-enhanced Raman scattering of methylene blue adsorbed on cap-shaped silver nanoparticles. Chem. Phys. Lett. 447, 305–309.

Yin, B.-C., Liu, Y.-Q., Ye, B.-C., 2012. One-Step, Multiplexed fluorescence detection of microRNAs based on duplex-specific nuclease signal amplification. J. Am. Chem. Soc. 134, 5064–5067.

Zhang, H., Liu, Y., Gao, J., Zhen, J., 2015a. A sensitive SERS detection of miRNA using a label-free multifunctional probe. Chem. Commun. 51, 16836–16839.

Zhang, H., Liu, Y., Gao, J., Zhen, J., 2015b. A sensitive SERS detection of miRNA using a label-free multifunctional probe. Chem. Commun. 51, 16836–16839.

Zhang, Y., Zhang, C.-Y., 2012. Sensitive detection of microRNA with isothermal amplification and a single-quantum-dot-based nanosensor. Anal. Chem. 84, 224–231.

Zhou, W., Tian, Y.-F., Yin, B.-C., Ye, B.-C., 2017. Simultaneous surface-enhanced Raman spectroscopy detection of multiplexed MicroRNA biomarkers. Anal. Chem. 89, 6120–6128.